Received: 22 January 2024 | Accepted: 18 November 2024

DOI: 10.1111/1365-2478.13648

Geophysical Prospecting | EAGE EUROPEAN ASSOCIATION OF GEOSCIENTISTS & ENGINEERS

ORIGINAL ARTICLE

Broadband seismic data acquisition and processing of iron oxide deposits in Blötberget, Sweden

Lea Gyger[1] | **Alireza Malehmir**[1] | **Musa Manzi**[2] | **Lilas Vivin**[3] | **Jean Lépine**[3] | **Ayse Kaslilar**[1] | **Oleg Valishin**[3] | **Paul Marsden**[4] | **Ronne Hamerslag**[4]

[1]Department of Earth Sciences, Uppsala University, Uppsala, Sweden

[2]School of Geosciences, University of the Witwatersrand, Johannesburg, South-Africa

[3]Sercel, Carquefou, France

[4]Nordic Iron Ore, Grängesberg, Sweden

Correspondence
Lea Gyger, Department of Earth Sciences, Uppsala University, Uppsala, SE 75236, Sweden.
Email: lea.gyger@geo.uu.se

Funding information
ERA-MIN 3, Vinnova, Grant/Award Number: 2022-00073; Swedish Foundation for Strategic Research, Grant/Award Number: CMM22-0003

Abstract

In June 2022, an innovative seismic survey was conducted in Blötberget, central Sweden, to evaluate the effectiveness of employing both a broadband seismic source and broadband receivers for mineral exploration in a challenging hardrock setting. The Blötberget mine hosts high-quality iron oxides, predominantly magnetite and hematite, sometimes enriched with apatite. These deposits comprise 10–50 m thick sheet-like horizons with a moderate eastward dip (~45°) along an NNE-trending zone. The survey employed a combination of co-located micro-electromechanical sensors, three-component recorders, surface and borehole distributed acoustic sensing, along with a 77-kN broadband seismic vibrator operating with 2–200 Hz linear sweeps. A tailored processing workflow was applied to preserve the broadband nature of the recorded data, and a one-dimensional velocity model was derived from the borehole distributed acoustic sensing data for migration and time-to-depth conversion purposes. Compared to the previous seismic surveys, the resulting seismic cross section reveals several well-defined reflections with improved resolution. Notably, a reflection intersecting the main deposits at a depth of approximately 1200 m exhibits a distinct polarity reversal relative to the reflection from the mineralization, providing further evidence for its interpretation as originating from a fault zone. Shallow reflections align with geological boundaries and partially coincide with weak magnetic anomalies. Additional reflections were revealed underneath the known mineralization on both sides of the fault zone and may suggest the presence of potential additional resources. The delineation of these reflections and the fault zone is critical for future mine planning and development in the region. This case study underscores the potential of broadband data in achieving high-resolution subsurface imaging in hardrock environment and its pivotal role in mineral resource assessment processes.

KEYWORDS
broadband, fault, mining, mineral exploration, seismics, data processing, imaging

INTRODUCTION

The Blötberget mine is located in the Bergslagen mining province in central Sweden. There, the ore consists of high-quality iron oxides in the form of magnetite and hematite partly enriched with apatite. The mineralization occurs in sheet-like horizons with a moderate eastward dip along an NNE-trending zone (Nordic Iron Ore, 2011). Bergslagen is a mineral province endowed with a wide range of deposits and has historically contributed to the wealth of industry in Sweden (Stephens et al., 2009). In Blötberget, like elsewhere in Bergslagen, mining operations were put to a halt in the late 1970s after the decline in iron ore prices worldwide. However, increasing demand and rising prices of raw materials and the presence of REEs (rare-earth elements) in the area have led to a new assessment of the mining potential of these apatite-bearing iron oxide deposits. After securing a mining concession for the area in 2011, Nordic Iron Ore conducted a series of feasibility and exploration studies in collaboration with several institutions to assess the mineable resources and gain further knowledge on the geological structures (e.g., Maries et al., 2017; Malehmir, Maries, et al., 2017; Papadopoulou et al., 2020). Given the deeper resources in the area (>500 m) and due to great density contrast with their host rocks (hence acoustic impedance contrast), reflection seismic methods were given a priority to be tested in the area.

Reflection seismic methods have proven to be a suitable tool for mineral exploration in hardrock environments (Malehmir et al., 2012 and references therein). The contrasting density of the ore body (approximately 4000–4500 kg/m^3) with regard to the host rock (approximately 2700–2850 kg/m^3) enables its detection using seismic methods and also allows for imaging key geological structures that may have implications for mine planning and the emplacement of the deposits (e.g., fractures and faults). Several seismic studies have so far been conducted in the area for methodological and technological testing given the wealth of borehole data available for validation. These have also provided valuable subsurface information such as indication for a lateral extension of the ore for 300 m beyond borehole data, the depth extension of the mineralized horizon down to approximately 1200 m depth from the known 800 m depth and the discovery of potential additional resources underlying the known deposits (Markovic et al., 2020; Malehmir et al., 2021). Another important finding from these seismic studies is the imaging of a reflection cross-cutting the mineralization with an opposite dip (e.g., Markovic et al., 2020; Malehmir et al., 2021; Pertuz et al., 2021) that has been speculated to correspond either to a mineralized zone or to a fault zone. In the latter case, the mineralization would be truncated at their intersection and could possibly continue in the footwall, albeit having potentially been subject to additional displacement. The interpretation of this reflection as a fault zone has been favoured so far due to the opposite dip with respect to the main mineralization and lack of reflection of the latter at a depth greater than 1200 m. Understanding the origin of this cross-cutting reflection and its relation with the mineralized horizons through improved imaging is important for both exploration and upcoming mine planning work in the area.

None of the previous seismic studies suggest any evidence of displacement along this potential fault nor were any kinematic studies done for the justification of any fault from the reflection data analysis. A topographic lineament southwest of Klenshyttan hints at the presence of a fault system associated with the opposing reflection cross-cutting the mineralization reflections (Malehmir et al., 2021). The need for additional constraints on this cross-cutting reflection led to the acquisition of a new set of seismic data in June 2022. To increase the resolution and depth extent of the seismic images compared to the previous studies, a combination of a broadband source with broadband receivers was used. The data were acquired along the same profile as the survey from 2019, where the signal from a broadband source was recorded by 10-Hz geophones (Pertuz et al., 2021).

Increasing the bandwidth of the recorded data offers several advantages. The benefits of generating and recording low frequencies include reduced wavelet side lobes of the seismic signal and a lesser sensitivity to scattering and attenuation. On the other side, high frequencies provide a sharper wavelet, hence enabling the resolvability of closely spaced seismic reflections. Broadband data therefore lead to improved subsurface imaging of both shallow and deeper geological structures (Ten Kroode et al., 2013). Some work has been presented to justify broadband seismic data acquisition as opposed to the conventional limited bandwidth seismic data in Blötberget (Pertuz et al., 2021) and at the Moab Khotsong Gold Mine in South Africa (Manzi et al., 2018). However, the literature on the use of broadband data in hardrock settings is scarce and more case studies and how-to solutions are required to bring this to an industrial standard.

The knowledge acquired from the numerous previous seismic surveys makes Blötberget the best seismically studied site in Sweden for technology testing and development works (Malehmir et al., 2023). This site is currently considered as an attractive location for development work in the frame of the Smart Exploration Research Centre (Malehmir et al., 2024). The extended knowledge of the area allows for the assessment of how the full broadband data can improve our understanding of the subsurface in a hardrock environment. The current study aims at (1) investigating the benefits of a full broadband seismic data acquisition in a hardrock environment and developing a tailored workflow for its processing, (2) providing further knowledge on the extent of the mineralization at depth, while (3) testing the fault hypothesis for the reflection cross-cutting the mineralization at 1200 m depth and (4) providing tools for mineral exploration that meet the needs of our society in the transition to green technologies and energy.

MICRO-ELECTROMECHANICAL SYSTEMS AND DISTRIBUTED ACOUSTIC SENSING

Both geophones and micro-electromechanical systems (MEMS) accelerometers are sensors made to record ground motion; geophones in velocity while MEMS in the acceleration domain. The difference comes from their construction characteristics. Geophones contain a spring-mounted coil, which remains stable while a fixed magnet moves along with the sensor casing in response to ground motion. The geophone sensor thereby generates an analog output signal in voltage proportional to the ground velocity and displays a relatively flat response to ground velocity above its resonance frequency whilst the amplitude of lower frequencies is significantly damped (Hons et al., 2008). MEMS, on the other hand, are digital electromechanical sensors with a lightproof mass that moves along with the casing and oscillates when changes in acceleration occur, providing a digital output proportional to the displacement of the proof mass (Mougenot et al., 2011). The absence of a coil–magnet system makes MEMS insensitive to electromagnetic noise. MEMS accelerometers have a linear amplitude and phase response below their resonance frequency (typically up to 1 kHz) down to 0 Hz (Hons et al., 2008; Mougenot & Thorburn, 2004). Additionally, MEMS are usually smaller and lighter than geophones with a digitizing unit making them easier to handle in the field and are more stable with respect to temperature and ageing of their components, providing more reliable seismic amplitudes and wavelet phase at low frequencies (Tellier & Lainé, 2017). Despite their higher cost (Brodic, 2017), MEMS are a valuable alternative to geophones.

Distributed acoustic sensing (DAS) is a technology based on the backscattered portion of laser pulses travelling through a fibre-optic cable. DAS behaves as a continuous sensor, which yields measurements of dynamic strain rate at densely spaced points along the fibre. Phase changes in the Rayleigh scattering of the laser pulse between two points separated by the gauge length can be related to the longitudinal strain applied on the cable by the seismic wavefield (Hartog, 2017; Kuvshinov, 2016). The inherent directional sensitivity of DAS can be counteracted by using a helically wound fibre optic cable, where the wrapping of the fibre around a thicker core increases its sensitivity to broadside waves (Kuvshinov, 2016). DAS systems act as broadband sensors for the properly selected gauge length (Cuny et al., 2020; Willis, 2022).

DAS has proven to be well suited for borehole applications such as reservoir characterization and monitoring of carbon capture and storage sites (e.g., Correa et al., 2017; Correa et al., 2021; Daley et al., 2016; Götz et al., 2018). A few studies have also shown the potential of DAS in mineral exploration, especially for vertical seismic profiling purposes (Bellefleur et al., 2020; Riedel et al., 2018), though examples of DAS applications for mining and exploration are still relatively scarce (Li et al., 2021).

GEOLOGY OF THE STUDY AREA AND PREVIOUS SEISMIC STUDIES

The host rock in the Bergslagen mineral province mainly consists of intermediate to felsic meta-volcanic rocks of Svecofennian age (1.91–1.88 Ga) likely formed in a back-arc-related tectonic setting (Allen et al., 1996). Mineralization in Bergslagen is mainly of Kiruna-type deposits (magmatic or high-temperature hydrothermal) with occurrences of smaller banded-iron- and skarn-iron-type deposits, mostly occurring as inliers within the volcanic rocks (Allen et al., 1996). According to a recent study, some of the iron oxide deposits were formed through magmatic precipitation within a larger volcanic superstructure, accompanied by hydrous alteration from a shallower hydrothermal system and low-temperature fluid circulation (Jonsson et al., 2013). Both the host rock and the apatite-iron-oxide mineralization underwent ductile deformation and low- to medium-grade metamorphism during the Svecokarelian orogeny (1.85–1.80 Ga) (Stephens et al., 2009), meaning that original structures and texture are difficult to recognize.

While the majority of the host rock in the Bergslagen mineral province exhibits SiO_2-rich dacites to rhyolites, the host rocks of Blötberget consist of andesites and dacites, indicating a more intermediate composition. The Ludvika region is characterized by a complex fold with a northeast-southwest fold axis. Mafic dykes, sills and pegmatites intersect both the deposits and the host rock. These late intrusions and their relationship with the mineralization are still a subject for detailed studies and may hold information on compactional changes and rare-earth elements (REEs) in the area. The ore forms sheet-shaped bodies consisting of magnetite and hematite and is accompanied by small amounts of quartz and calc-silicate minerals. The presence of apatite is also relevant since this critical raw material can also be enriched with REEs and makes the iron oxide deposits in Bergslagen even more important for mining in this era of energy transition. The sheet-like units of 10–50 m thickness are inclined towards the southwest with a dip of approximately 45° until 500 m depth, where the dip becomes gentler. As of today, the mineralization is expected to extend down to 1200 m depth, where the cross-cutting reflection interrupts its continuity (Malehmir et al., 2021).

The mining history in the Ludvika area dates back to the 16th century. Prior to its closure in 1979, Blötberget was mined down to 240 m depth using underground mining methods. Nordic Iron Ore plans to restart the mining operations at 420 m below the mined-out areas (Nordic Iron Ore, 2011). In

2015 and 2016, tests were conducted to optimize the metallurgical concentration of the ore and established the possibility of preparing products with an average iron concentration close to 69%, making it one of the highest iron-ore qualities in the world. As of today, the available mineable resources are estimated at 55.1 Mt with an average grade of 40.7% Fe and a cutoff grade of 25% Fe, the magnetite-hematite proportion being 62:38 (Nordic Iron Ore, 2019).

During the period under which the mine was active, ground-based geophysical surveys were conducted during the 1950s. Airborne geophysical surveys including magnetics were conducted in the 1970s, and core drilling was conducted from 1942 to 1977. As a consequence of new mining permits for Blötberget, a new set of exploration activities started in 2011. A series of new boreholes were drilled, and several studies comprising varying geophysical techniques were conducted. The results from two gravity surveys in 2015 and 2016 were compared to the aeromagnetic data from 1972 (Yehuwalashet & Malehmir, 2018). Rock magnetic measurements were carried out on drill core material and hand specimens (Almqvist et al., 2019). Maries et al. (2017) investigated physical properties and rock quality of the host rock and ore using downhole logging of seven boreholes intersecting the mineralization. A UAV (unmanned aerial vehicle) magnetic survey successfully detected two distinct mineralized zones of magnetite and hematite (Malehmir, Dynesius, et al., 2017) and led to follow-up UAV-based instrumentation work (Bastani & Johansson, 2022).

Pilot two-dimensional (2D) reflection seismic profiles were acquired in 2015 and 2016 with a combination of a seismic landstreamer (micro-electromechanical sensors based), cabled-based and wireless recorders connected to geophones and a 500-kg drophammer mounted on a small skid-steer loader alongside 30 explosive shots of approximately 50–100 g as seismic sources (Malehmir, Maries, et al., 2017; Maries et al., 2020; Markovic et al., 2020). These studies hinted at an approximately 300 m extension of the mineralization at depth, which was later confirmed by the results of a sparse three-dimensional (3D) survey completed in 2019 (Hloušek et al., 2022; Malehmir et al., 2021). These seismic datasets have also been used to test and improve data processing methods, such as surface-wave analysis for static corrections (Papadopoulou et al., 2020), prestack depth imaging techniques (Bräunig et al., 2020), reverse time migration (Ding & Malehmir, 2021) and surface-wave suppression through seismic interferometry (Balestrini et al., 2020). The outcome of the 3D seismic survey suggested a lateral extension of the deposits of 300 m towards the west with potential additional resources of 10 Mt to the previously estimated resources (Malehmir et al., 2021). The 3D study also highlighted two major sets of reflections cross-cutting the mineralization with an opposite dip angle. These reflections were interpreted to have an accumulated reverse fault component, possibly terminating the deposits at depth.

Finally, a new set of seismic data was recorded in September 2019 (Pertuz et al., 2021) to validate the suitability of a broadband electromagnetic vibrator (E-Vib) with a peak force of 7 kN for seismic imaging in hardrock environment (Noorlandt et al., 2015). The 2–180 Hz seismic signal was recorded by 4.5- and 10-Hz geophones, and a custom-processing workflow was presented to retain the broad bandwidth of the data. The results of this survey demonstrated how using a broadband source could increase the signal quality and data resolution. However, given the limited bandwidth recorded by geophones, a new dataset with broadband receivers was required to improve the resolution further.

SEISMIC DATA ACQUISITION

In June 2022, new seismic data were acquired along a gravel road crossing a swampy forest with a section of asphalt road on the southern third portion of the profile. The seismic profile covered the same 2D survey profile that was conducted in 2019 and the earlier studies of 2015 and 2016 (Markovic et al., 2020; Pertuz et al., 2021), although being slightly shorter on the southern end (Figure 1).

The surface receiver array consisted of 492 single-component micro-electromechanical sensors (MEMS)-based nodal recorders with 5 m spacing, partly co-located with 150 10–Hz 3C geophone-based recorders with 10 m spacing and a 2200 m long straight surface distributed acoustic sensing (DAS) cable (Figure 2). The surface DAS cable consisted of a single-mode, straight telecommunication fibre that was not trenched but covered with gravel to improve its coupling to the ground. An additional 460 m long DAS single-mode helically wound cable (HWC) was deployed in an uncased borehole located 100 m away from the surveyed profile. The borehole, originally 650 m long, was blocked at 460 m depth, almost ~~a~~ 100 m above the mineralization. Starting straight but quickly deviating towards the ore, the borehole was naturally filled with water and was not cemented after the placement of the fibre to allow for future downhole logging. The coupling of the slacking HWC to the borehole wall was likely improved by the fact that the borehole was inclined. The interrogator unit was set to use a 10 m gauge length with 5 m spatial sampling for both cables. The DAS data were acquired continuously, and the shot records were extracted after the survey was completed. A constant time shift was observed in the DAS data with respect to the GPS clock of the shot-triggering system and was corrected for when extracting the relevant data from the continuous recordings. The MEMS used in this survey are accelerometers capable of recording a seismic signal with a bandwidth of 0–400 Hz, at a sampling rate of 1 ms. Final receiver and shot positions were assigned by combining differential global positioning system (DGPS) measurements with national LIDAR (laser imaging, detection and ranging)

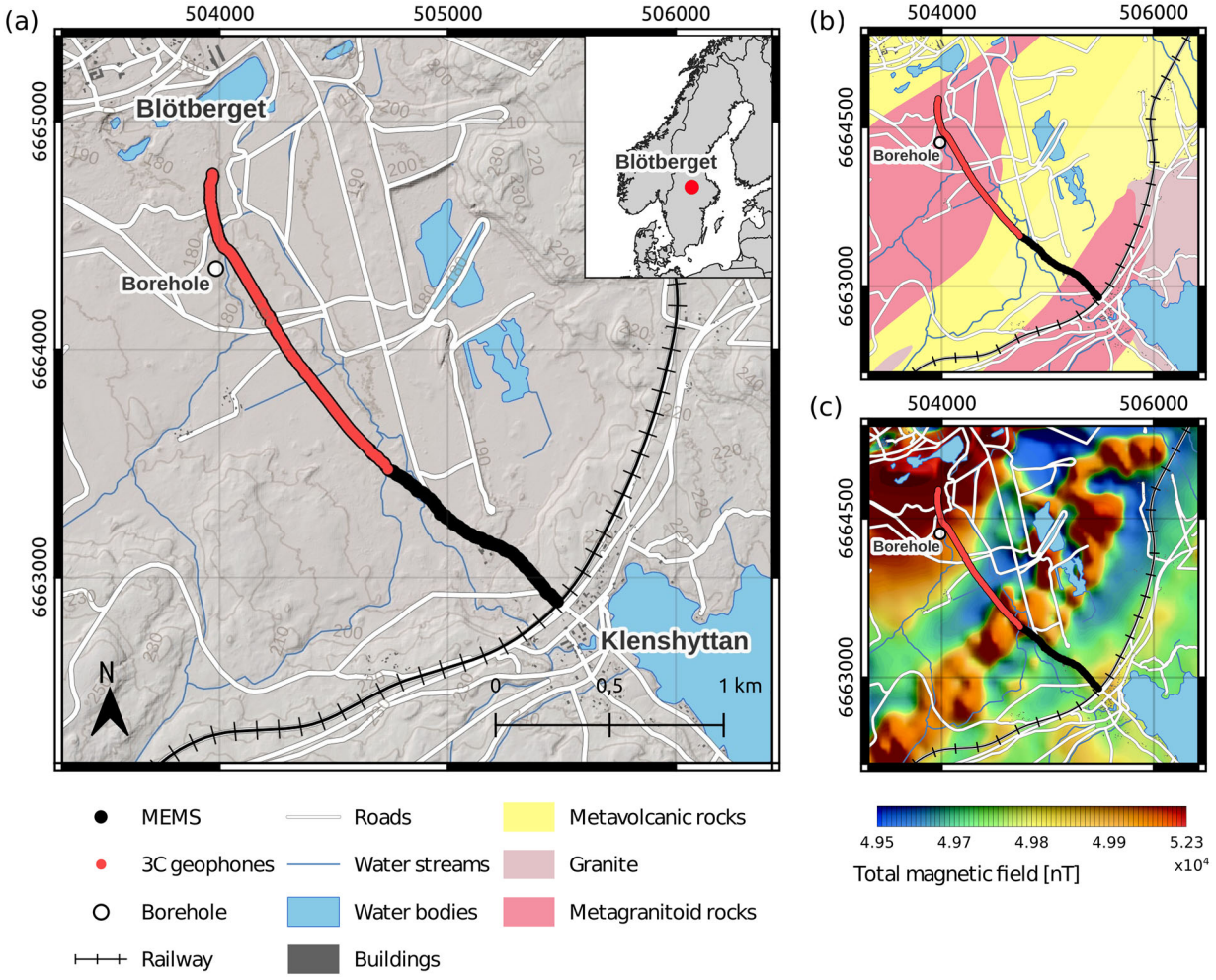

FIGURE 1 (a) The study area and the location of the seismic profile from 2022 with the MEMS-based receivers in black and co-located geophone-based receivers in red. A distributed acoustic sensing helically wound cable (HWC) was instrumented in a borehole located 100 m from the profile. The HWC recorded shots generated along the surface profile. (b) Geological map of the Blötberget area, modified from the Geological Survey of Sweden (SGU, 2018). (c) Airborne magnetic map from the SGU database.

data to compensate for poor DGPS data quality where the forest cover was too thick. While these various seismic recorders were used as part of a technology and how-to solution testing, this study focuses on the data recorded by the MEMS and uses first-break arrivals recorded by the HWC DAS cable to generate a 1D velocity model for migration of the MEMS data.

A seismic vibrator (Nomad 15) with a peak force of 77 kN was used as the vertical seismic source. Three sweeps were performed by the source at every receiver location (5 m spacing), using a linear 18 s long sweep of 2–200 Hz at 70% of the vibrator's peak force. The number of sweeps was increased up to 10 at the shot points located closest to the borehole, forming a near-offset vertical seismic profiling record. The acquisition parameters are summarized in Table 1.

TABLE 1 The 2D seismic data acquisition parameters of the 2022 survey in Blötberget.

Parameter	Comment	
Geometry	Fixed	
Profile length	2500 m	
Direction	NW-SE	
Receivers	500 MEMS	5 m spacing
	150 3-C 10 Hz geophones	10 m spacing
	Straight DAS (surface)	2200 m
	HWC DAS (borehole)	460 m
	DAS gauge length	10 m
	DAS channel spacing	5 m
	Sampling rate	1 ms
Source	Nomad 15	77 kN peak force
Sweep	2–200 Hz, linear, 18 s	5 m shot spacing

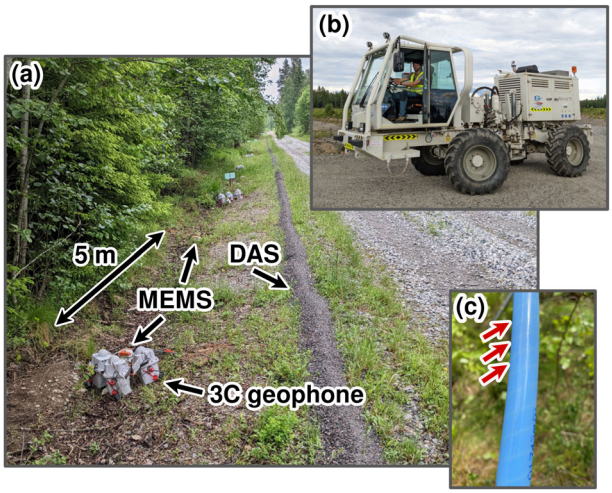

FIGURE 2 Field photographs showing (a) the acquisition set-up on the surface with micro-electromechanical sensors (5 m spacing) and three-component geophones (10 m spacing) collocated with the straight distributed acoustic sensing (DAS) cable covered with gravel. (b) The seismic source, a seismic vibrator (Nomad 15) with a peak force of 77 kN and (c) the DAS helically wound cable placed in the borehole BB12010, close to the acquired seismic profile, with the red arrows pointing at the wrapped fibre inside the casing.

METHODOLOGY

The acquired seismic data were processed following a workflow that allowed their broad bandwidth to be retained as much as possible. The raw data were first cross-correlated with the theoretical sweep from the vibrator to yield the shot records. The repeated shot records at each shot location were then vertically stacked to increase the signal-to-noise ratio. Strongly reflected events could already be observed on the raw shot gathers (Figure 3a). The surface-consistent refraction static corrections were computed based on the first-break picks and a two-layer model with a final root mean square error of 2.45 ms. Both the short- and long-wavelength portions of the solution were applied to the data. This step significantly improved the continuity of the reflected events. An airwave filter was then applied with a velocity of 330 m/s (Figure 3b).

The next processing step involved filtering out surface waves (SW) using a tailored workflow. Given the dominant low-frequency and high-amplitude nature of SW, a bandpass and/or spectral equalization filter is conventionally applied for this purpose. However, given our interest to retain the bandwidth, a new approach was developed. This methodology assumes a low dispersion for the SW, as observed in Blötberget (Papadopoulou et al., 2020) and most hardrock sites. Additionally, the limited thickness of the top soil layer to a maximum of 20 m (SGU, 2014) prevents SW from becoming significantly dispersive. The idea behind this workflow is simple: the surface waves are aligned in order to be removed more effectively.

The first step of this methodology involves stacking SW to increase their signal and calculating the residual static corrections to align them. To begin with, we applied a bulkshift of 1000 ms followed by a linear moveout (LMO) correction of 2100 m/s on the shot gathers to bring the SW horizontally. The shot gathers were then stacked, yielding a stacked seismic section with strong horizontal events (Figure 4a). One round of surface-consistent residual static correction was then calculated on this stacked section focusing on the time window between 1000 and 1100 ms, resulting in a receiver-shot-based solution for the SW static corrections (Figure 4b).

Going back to refraction static corrected shot gathers (Figure 5a), we applied our SW residual static corrections, thus improving the alignment of SW (blue boxes in Figure 5b). A bulkshift of 1000 ms and an LMO correction of 2100 m/s were performed on the shot gathers. The horizontal SWs were then removed from the shot gather using a horizontal median filter. Subsequently, an inverse LMO correction and inverse bulkshift were applied to the shot gathers to bring them back to their original form (Figure 5c). Finally, the SW residual static correction was removed from the data, leaving a dataset clear of SW (Figure 5d). The improvement of this method compared to a simple median filter with a constant velocity of 2100 m/s to remove SW on our data is limited, probably due to its high fold. Nevertheless, this tailored workflow provided slightly better results and was therefore applied to our dataset (Figure 3c).

The remaining source-generated and ambient noise was successfully attenuated by a gapped deconvolution filter with a gap length of 8 ms and a filter length of 150 ms. This filter was particularly effective in suppressing some noise considered to originate from the source (Figure 3d). Prior to the reflection residual static calculation, a bandpass filter (10-40-110-130 Hz) and spectral equalization (20-50-100-120 Hz) were applied to the data. The goal here was to obtain a clear reflection from the mineralization and therefore provide a more accurate solution for the residual statics. The residual static solution was completed after two rounds of calculations looped with the velocity analysis. The bandpass and spectral equalization filters were then removed prior to the application of the residual statics, hence retaining the data bandwidth from the acquisition. To resolve the conflicting dips of the mineralization and the cross-cutting reflection, a Kirchhoff dip moveout (DMO) correction was performed on the data. The DMO correction improved the geometry of the mineralization M1–M3 as well as the strength of the reflections from R1 to R4 (Figure 6). Additionally, a diffraction hyperbola with its apex at 400 ms around CDP 610 became more apparent.

Post-stack processing work involved the use of FX-deconvolution and trace balance to improve the coherency of the reflections. Finally, the seismic section was migrated using

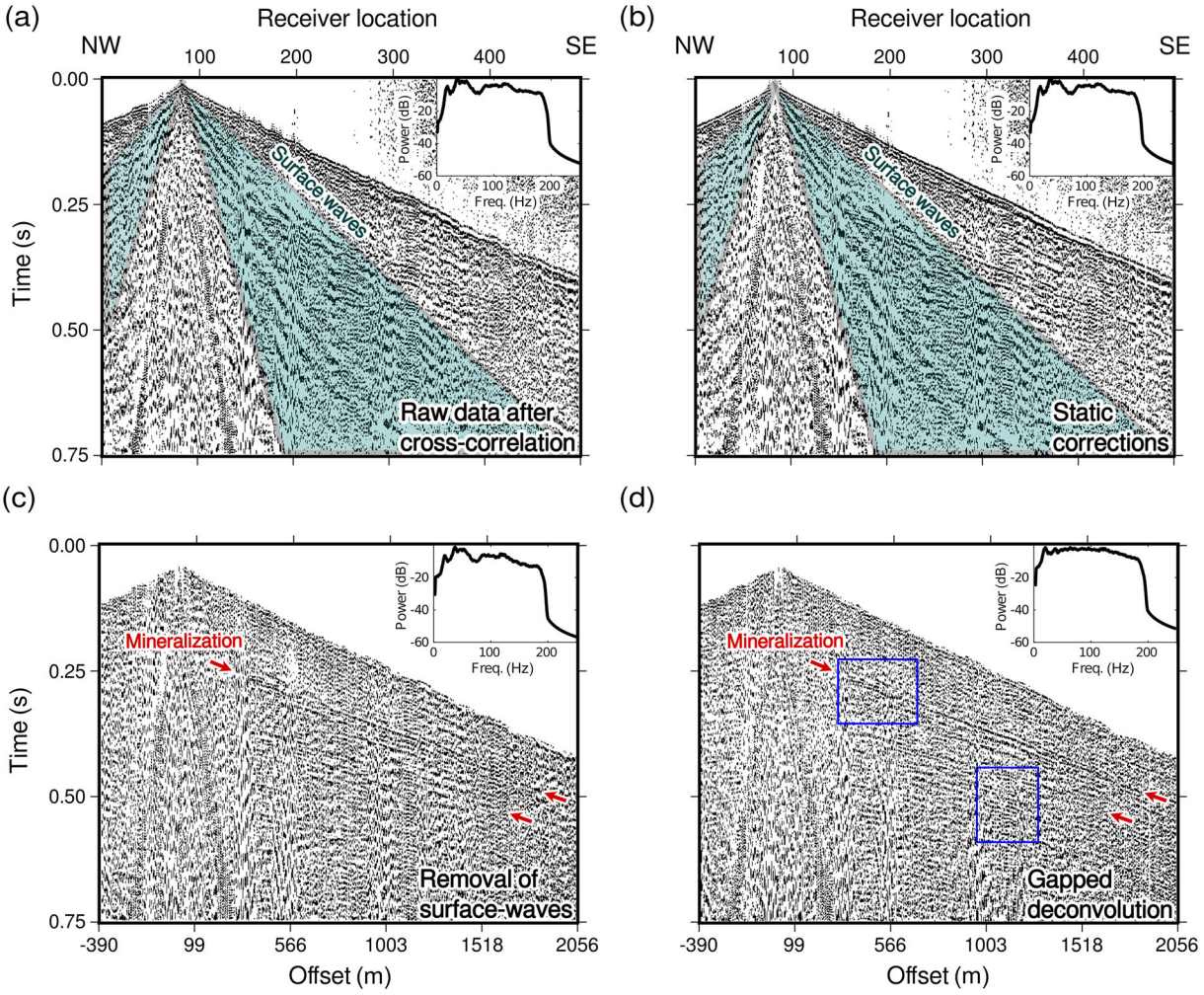

FIGURE 3 (a) An example of a raw shot gather cross-correlated with the 18 s theoretical sweep, (b) with refraction static corrections and an airwave filter applied, (c) after the removal of surface waves and (d) gapped deconvolution. The surface waves are highlighted in the light blue regions. The red arrows point at the reflections from the mineralization, and the dark blue boxes highlight the improvement after the implementation of the gapped deconvolution.

the phase-shift method and a 1D velocity model extracted from the helically wound fibre optic cable (HWC) placed in the borehole. This migration method was selected based on its ability to handle steeper reflections.

To construct the 1D velocity model from the borehole data, the repeated shot records of the shot point located closest to the borehole were extracted from the DAS HWC, thus producing a near-offset vertical seismic profiling. The constant time delay in the DAS data was corrected by using the data from a MEMS placed next to the entrance of the borehole. The HWC DAS records were converted from differential phase to strain and vertically stacked. The first-break arrivals were picked to compute the 1D velocity model (Figure 7a). Two different velocity gradients are visible in the calculated model (blue line in Figure 7b,c), suggesting the presence of a low-velocity layer from 0 to 300 m depth. The small changes in velocity were smoothed out by a simple line fit following those two gradients. To compensate for the absence of fibre cable below 460 m, velocity values were extrapolated to 2000 m depth following the second velocity gradient, giving a rough estimate of the velocity field at depth. Finally, this velocity model was used for the time-to-depth conversion. The processing steps followed in this study are summarized in Table 2.

RESULTS

The processing of the seismic data mainly focused on the top 750 ms, where the main reflections from the mineralization and the cross-cutting reflection are located. The migrated section (Figure 8) exhibits two major reflections, M1 and M2, whose geometries closely adhere to the modelled three-dimensional (3D) surface of the ore horizons. This ore model was derived from the sparse 3D survey (Malehmir et al., 2021) in conjunction with borehole data. A third reflection, M3, beneath these two primary reflections, follows the same

TABLE 2 Processing workflow and parameters applied to the broadband MEMS data.

Step	Process	Parameters
1	Data input	SEG-D format
2	Cross-correlation	With theoretical sweep
3	Vertical stack	Vertical stack of repeated shots to increase S/N
4	Geometry	Correction and interpolation for missing geodetic data
5	Trace edit	Killed noisy traces
6	First-break picking	Automatic and manual
7	Refraction statics	Two-layer model using surface elevation and first breaks
8	Airwave	Linear attenuation at 330 m/s
9	Gapped deconvolution	Gap length: 8, filter length: 150 ms
10	Bandpass	10-40-110-130 Hz, removed later
11	SPEQ	20-50-100-120 Hz, removed later
12	Surface waves removal	Tailored surface waves removal scheme
13	Residual statics	Surface-consistent (iterative, 2 rounds)
14	Trace muting	Mute first breaks and above
15	AGC	Window length: 250 ms
16	DMO	Constant velocity: 6000 m/s
17	NMO	Dip-independent velocity model
18	Stack	2.5 m CDP spacing
19	FX-decon	Filter length: 19 traces, window length 100 ms
20	Balance	Trace scaling relative to absolute amplitude
21	Migration	Phase-shift migration using 1D velocity model of near-offset HWC data
22	Time-to-depth conversion	Conversion using the same 1D velocity model as for migration

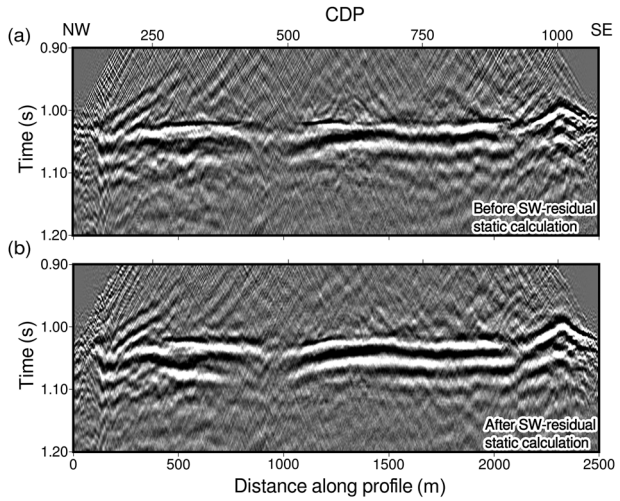

FIGURE 4 Stacked surface waves after being horizontally aligned on the shot gathers using a constant LMO velocity of 2100 m/s (a) before and (b) after computing one round of surface-consistent residual static corrections to align them better.

geometry. A set of further reflections (L1 and R1–R4) can also be observed in the section. While L1, R1 and R2 were present but partially interpreted in previous studies, reflections R3 and R4, located below F1 and M1–M3, respectively, are imaged in this study for the first time.

The cross-cutting reflection F1 intersects the mineralization at ~1200 m depth. This reflection, consistently identified in various earlier seismic studies in the area, is attributed to a fault. Upon closer examination of F1, the polarity of the reflection appeared different from that of other reflections in the seismic section. We performed a wavelet comparison between the signal of the first breaks in the shot gathers and this reflection on the unmigrated stacked section. We selected 30 traces containing the first-break signal at a near offset of one representative shot gather and aligned them after muting the noise above them (Figure 9a). Similarly, 30 CDP (common depth point) traces containing the reflection were chosen and aligned, with muting of the incoherent signal around it (Figure 9b). The results unequivocally demonstrate a polarity reversal from F1 with respect to the first breaks, hence justifying for the first time the presence of lower impedance material to generate this reflection response.

To provide a quantitative comparison of the recorded data quality from the micro-electromechanical sensors (MEMS) with the vertical component measurements of the 3C geophones, an analysis of the amplitude spectrum was conducted. This analysis specifically targeted the data acquired from shots recorded along the segment of the profile where the 3C

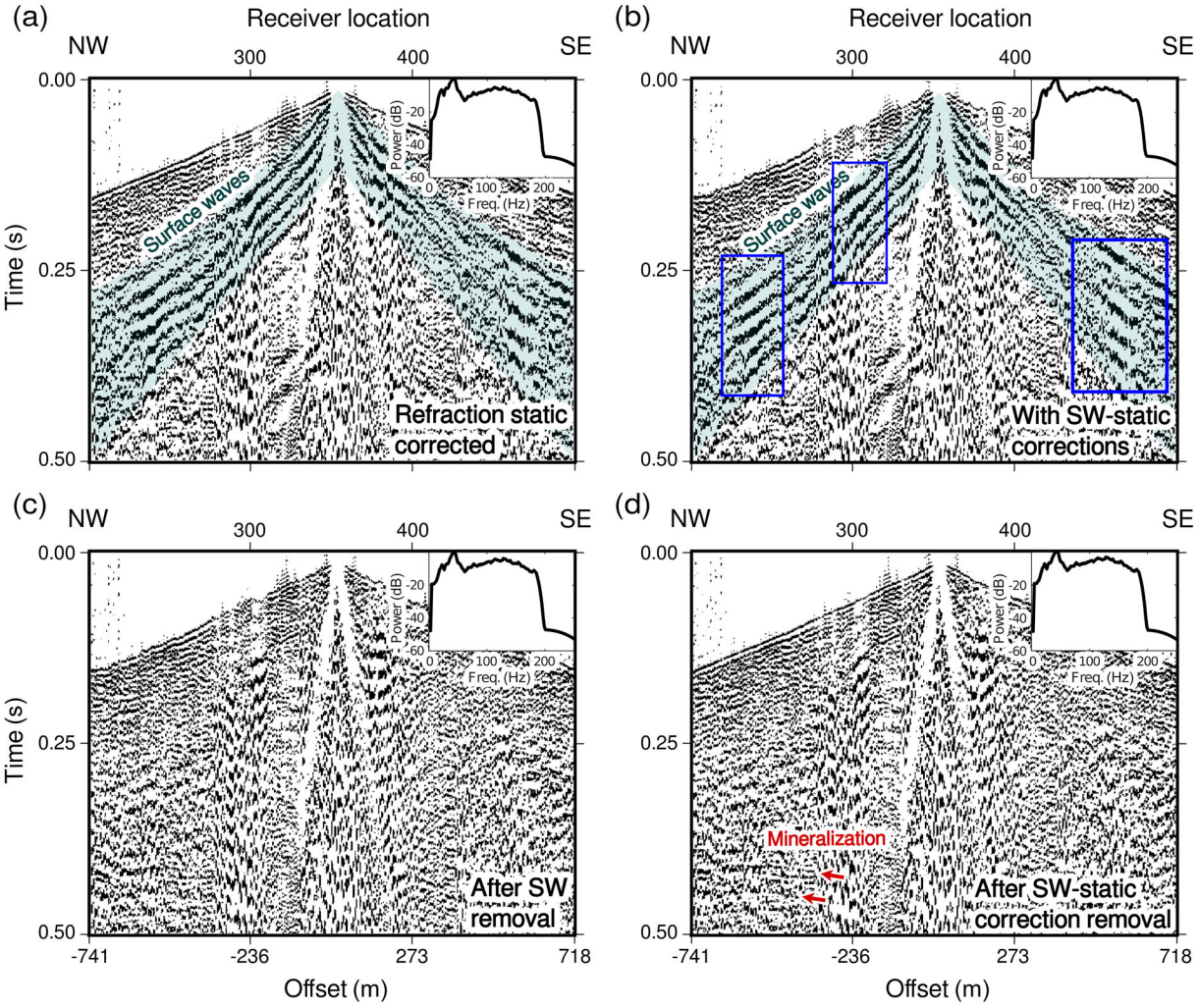

FIGURE 5 (a) Refraction static corrected shot gather before and (b) after surface-wave residual static corrections to align the surface waves. The improvement in the surface-wave alignment is highlighted by the blue boxes. (c) Removal of surface-wave energy using a median filter and (d) removal of the surface-wave residual static corrections, leaving an improved reflection signal from the mineralization (red arrows).

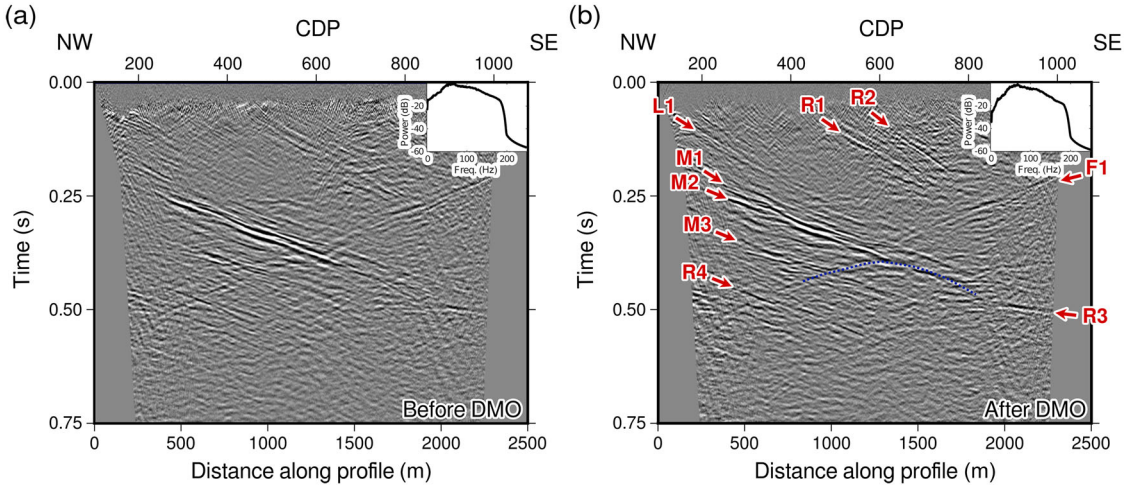

FIGURE 6 (a) Unmigrated stacked section before and (b) after DMO corrections. The use of DMO significantly improved the strength and continuity of the labelled reflections, especially in the case of R1–R4. The dotted dark blue line highlights a diffraction hyperbola with its apex located at the end of M2.

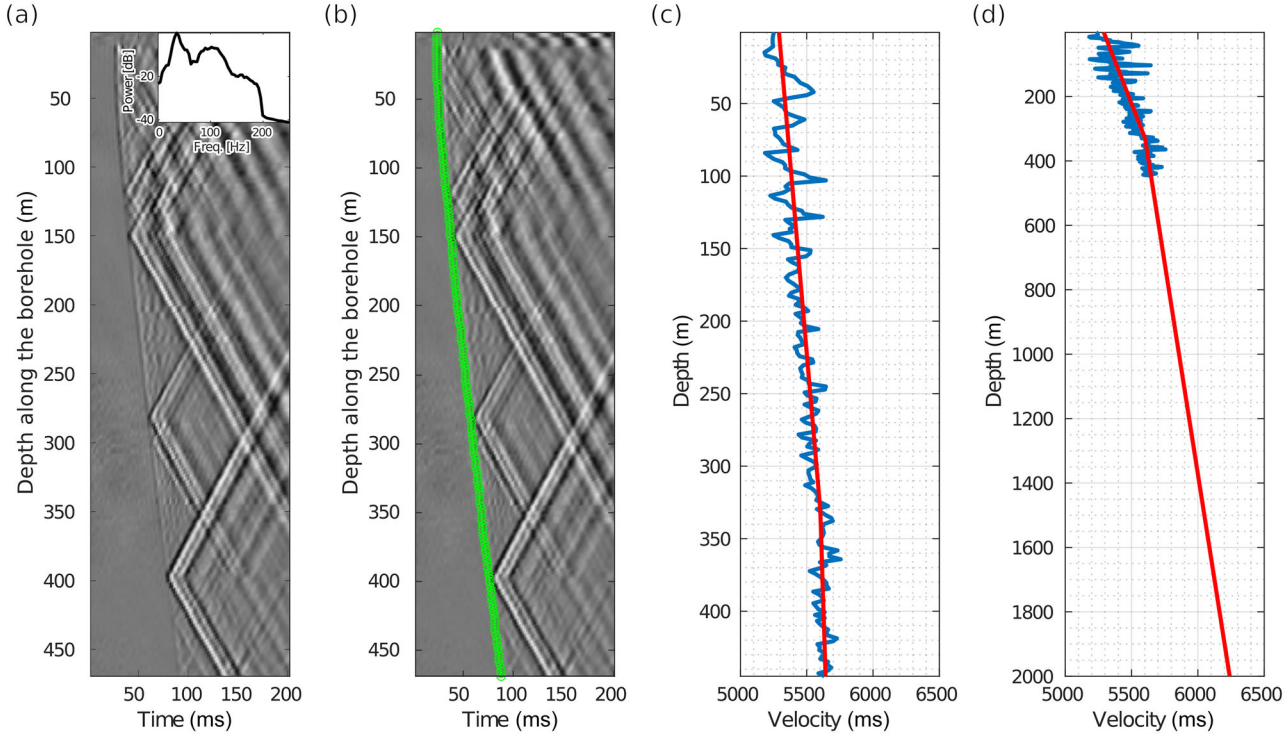

FIGURE 7 (a) Raw shot gather from the HWC DAS cable (b) with the picked arrivals in green and (b) derived 1D velocity model (blue line) as well as a two-layer velocity model (red line). (c) The two-layer velocity model was extrapolated up to a depth of 2000 m. The resulting velocities are in agreement with the values expected for P-waves in crystalline rocks of felsic to intermediate composition (Kearey et al., 2002).

receivers with geophones were deployed. The analysis was done on cross-correlated data with refraction static corrections only. The amplitude spectrum of the entire shot gather for every 10th shot position was calculated and subsequently averaged for each dataset, as illustrated in Figure 10. Given that MEMS record particle acceleration and geophones particle velocity, an additional step involved the integration of MEMS data into velocity (Figure 10b). The resulting amplitude spectra are shown in Figure 8a for the geophones and Figure 10b,c for the MEMS. Finally, the averaged spectra underwent normalization and are jointly presented in Figure 10d,e for comparison.

While acknowledging the importance of having both datasets corresponding to the same type of particle motion to provide a fair comparison (here with both MEMS and geophone data in velocity), an additional investigation was made to assess the quality of the recorded signal for both datasets in their original form. This time the datasets are compared with MEMS data in acceleration and geophone data in velocity since these are the types of particle motion both sensors are, respectively, designed to record and that are used for processing. To this end, the signal-to-noise (S/N) ratio was calculated on the shot gathers for the portion of the seismic profile where the 3C geophones were deployed. For the MEMS data, only the receivers co-located with 3C geophones were considered. The root mean square (RMS) amplitude of a time window above the first breaks containing exclusively noise was compared to that of a time window containing the first-break signal. The first breaks were shifted down by 200 ms and aligned using a linear moveout operator. Subsequently, a time window of 100–190 ms and 200–250 ms was selected for the noise and signal window, respectively, within an offset range of 550–1200 m. The mean value for the RMS amplitude of all traces within the designated time windows was computed for every shot, providing the S/N ratios. Finally, the S/N ratios of all shot gathers were averaged to yield a single value for each dataset. The calculated S/N ratios were 7.61 for the 3C geophones and 8.96 for the MEMS. The combination of these two approaches enables a systematic and quantitative evaluation of the spectral and signal quality characteristics, offering insights into the performance and coherence of data obtained from both sensor types.

DISCUSSION

The wealth of data from previous studies in Blötberget enables us to evaluate the performance of full broadband seismic data in a hardrock environment. This survey was the first to use the combination of a broadband source with broadband receivers in the study area, and one of the few studies on broadband data for land seismic acquisition reported in the literature in

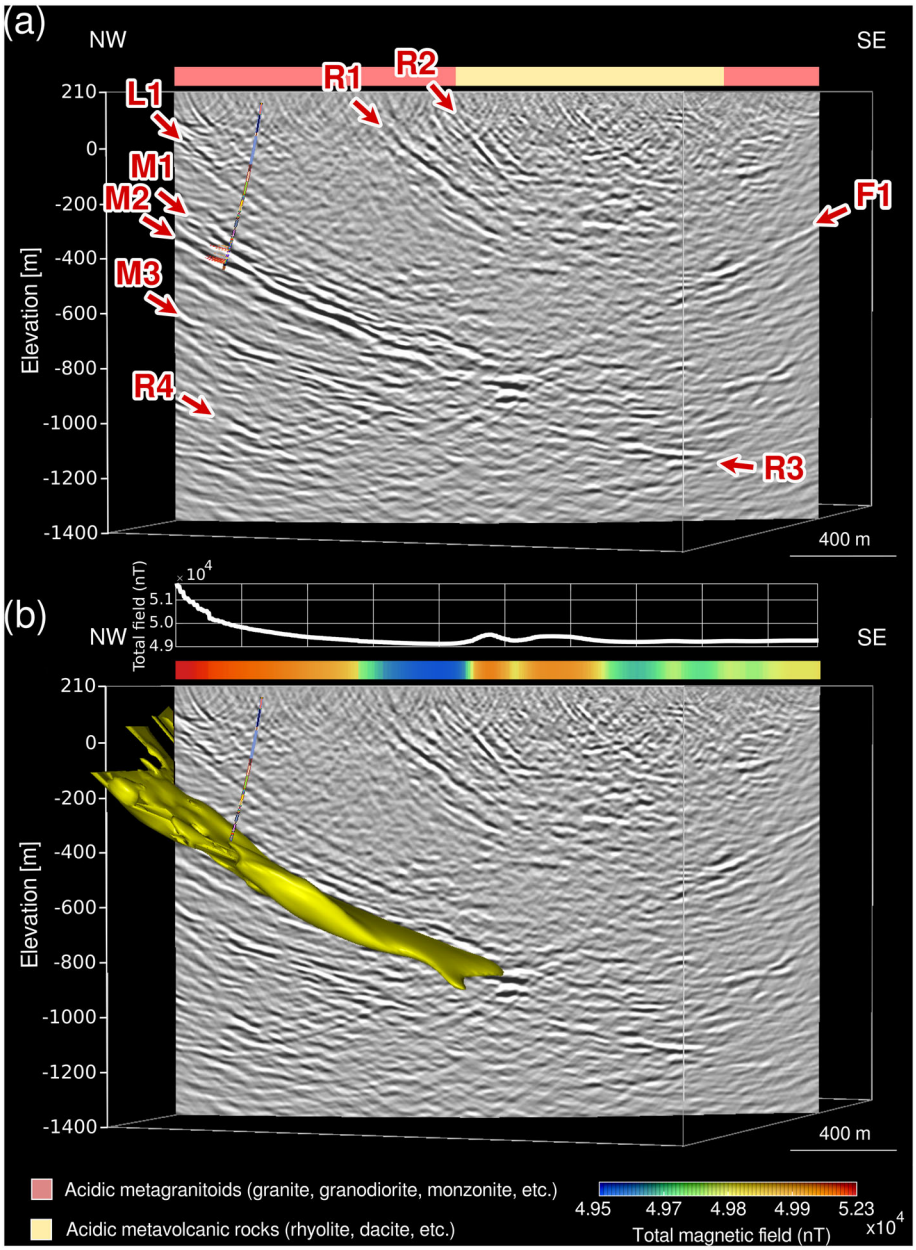

FIGURE 8 (a) Migrated and time-to-depth converted section with the identified reflections and location of the borehole where the DAS HWC was deployed. The geology strip above the seismic section was extracted from the geology map in Figure 1b, following the seismic profile. (b) Same section superimposing the ore model constructed based on borehole and 3D seismic data (Malehmir et al., 2021). The total magnetic field along the seismic profile is shown above the seismic section and presents the same data as in Figure 1c. The geological and magnetic data were extracted from the SGU database.

general (see also Denis et al., 2013; Manzi et al., 2018; Pertuz et al., 2021). Micro-electromechanical sensors (MEMS) are known to have technical advantages compared to geophones. These include being usually lighter, smaller, more energy-efficient, insensitive to electromagnetic-electric noise as well as being independent of temperature changes and less sensitive to the ageing of the components (Tellier & Lainé, 2017). Besides these field advantages, the data display a flat amplitude and phase response in the acceleration domain. With the co-location of MEMS and 3C geophones, this survey offers an opportunity to compare the quality of the signal recorded by the two types of sensors. Examining the amplitude spectra of both datasets (Figure 10a–c), one notices some variability in the shape of the amplitude spectrum for each record. These irregularities may be attributed to technical issues with the seismic source, and therefore inconsistencies in sweeping power, and/or to near-surface effects. However, it is noteworthy that this variability is consistent across both datasets, facilitating a direct comparison. The amplitude peak at 77 Hz, present in most shot gather, is likely source-related and

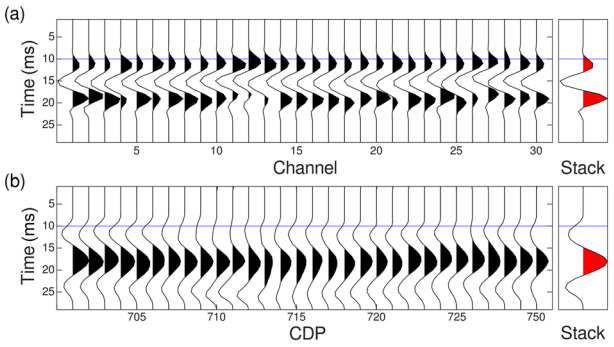

FIGURE 9 (a) Horizontally aligned first breaks from a shot gather and (b) aligned CDP (common depth point) traces from the stacked seismic section, showing the reflection cross-cutting the mineralization, with the red traces corresponding to their corridor stacks. Note the distinct polarity difference between the two features.

disappears at far offset. A general enhancement in energy recorded by the MEMS is observed for frequencies above 70 Hz (Figure 10b). Figure 10e illustrates the gain in the low frequencies of the MEMS dataset. Finally, the S/N ratio comparison further indicates an improvement in signal quality for data recorded by the MEMS.

This survey was also the first in the study area to combine simultaneous borehole data recordings with the surface seismic data acquisition. The survey capitalized on the presence of an open borehole near the profile. Because the borehole had to remain accessible and could not be cemented, the distributed acoustic sensing cable was quickly deployed and retrieved. Nevertheless, the data contained good quality first breaks, which were necessary to construct a velocity model. The extracted and subsequently smoothed velocity model yielded a reliable migrated section, aligning well with velocity values expected for P-waves in magmatic rocks of felsic to intermediate composition (Kearey et al., 2002). This study illustrates the utilization of nearby exploration boreholes for velocity measurements while ensuring their availability for subsequent logging activities.

The majority of the reflections depicted in the final seismic section (Figure 8) are consistent with findings from previous studies. This is the case for M1 and M2, which are known and interpreted to originate from the mineralization based on borehole data and their strong amplitudes. The presence of M3 has consistently been documented in several earlier studies (Maries et al., 2020; Markovic et al., 2020; Malehmir et al., 2021; Pertuz et al., 2021). Projecting M3 to the surface, the reflection plane intersects with a magnetic lineament, suggesting the presence of potential additional resources in the footwall of the mineralization.

The cross-cutting reflection, F1, was also identified in most of the previous studies. Malehmir et al. (2021) projected this reflection to the surface, where a topographic lineament can be observed and the presence of a lake. This reflection has traditionally been interpreted as a fault based on several observations; the lack of magnetic signature of this topographic lineament, the opposite dip of F1 relative to other reflections present in the seismic section, the interruption of the reflection from the mineralization at their intersection and the presence of a diffraction hyperbola, suggesting the truncation of the mineralization. The high-resolution data of this study exhibit the clearest signature from this reflection to date. As noted earlier, the polarity of F1 is reversed compared to that of the first breaks. When a P-wave is reflected at the interface with a material of lower acoustic impedance, a reversal in polarity is observed in the reflected wavefield (Nanda, 2021). Considering the relation between seismic impedance and rock density, we suggest that this reflection might correspond to the presence of a weak zone. Following this interpretation, either the damage zone around the fault needs to be wide enough to be imaged and/or the fault needs to be hydraulically conductive. Nevertheless, these findings provide further evidence for the interpretation of F1 to originate from a fault. Unfortunately, the current survey geometry hindered the investigation of the possible continuity of this reflection to the surface. Additionally, owing to the 2D nature of the survey, the complex geometry of the intersection between F1 and the mineralization proved difficult to resolve accurately due to additional out-of-plane signals.

L1 has previously been identified as a lithological contact between intrusive and volcanic rocks (Malehmir et al., 2021; Ding & Malehmir, 2021). With a similar geometry to that of the mineralization, indications of R1 and R2 were visible in earlier results (Ding & Malehmir, 2021; Markovic et al., 2020; Pertuz et al., 2021). R1 lacks correspondence with any known geological boundary or magnetic lineament. Conversely, a weak anomaly is evident on the magnetic data above R2, and the geological map indicates an additional lithological contact where R2 extends to the surface (Figure 10b). The precise nature of these two reflections remains uncertain but could potentially denote geological unit boundaries or, in the case of R2, a weaker (e.g., thinner) mineralized horizon. R3 and R4 are seen for the first time and are present both in the unmigrated and migrated sections. These two reflections are challenging to interpret due to the low seismic fold on each end of the profile, limiting our ability to track their potential continuation beyond the profile length, and leaving their overall geometry unclear.

Reflection R3 is particularly important when trying to understand the complex geological history in Blötberget. So far, the mineralization was thought to be truncated at ~1200 m depth and interrupted at the intersection with F1, with no sign of the mineralization in the footwall of the fault. However, the new seismic section may suggest a dominantly reverse fault associated with R3, implying that the mineralization in the footwall might be located only a few tens of metres down towards the south of the profile. These findings challenge the

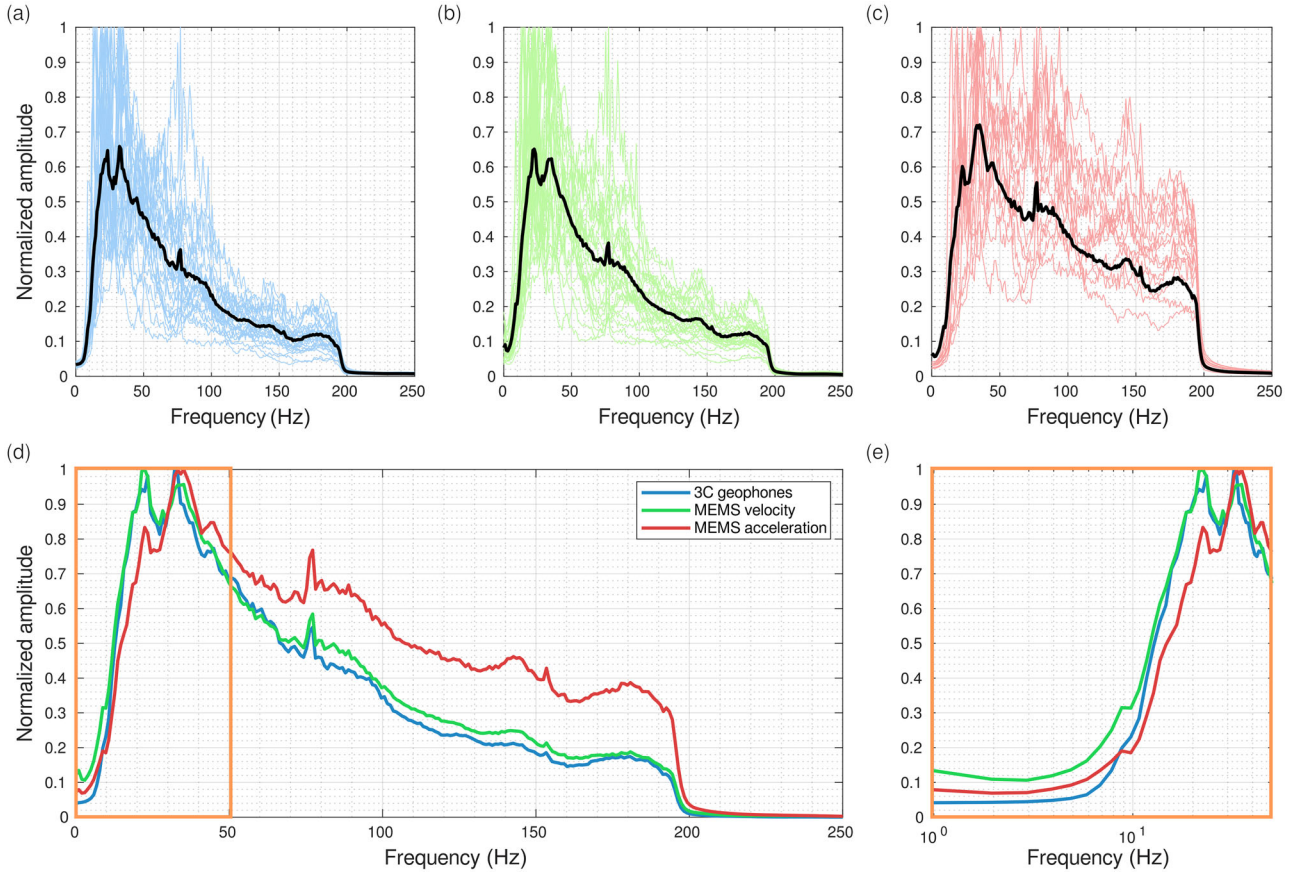

FIGURE 10 (a) Normalized amplitude spectra of every 10th shot gathers recorded by the vertical component of the 3C geophones in blue and average spectra in black. (b) Same amplitude spectra for the MEMS data in velocity in green and (c) in acceleration in red. (d) All three averaged spectra (a–c) are normalized and plotted together for comparison, (e) and focusing on 0–50 Hz using a logarithmic scale for better comparison of the corner frequencies on the lower end of the spectra.

current knowledge of the geological processes at play in this area and encourage further investigation into the deformation history of the region. Future surveys will benefit from extending the profile on its southern end with both receivers and shots to image the possible continuity of F1 to the surface and R3 at depth. This has not been possible given source permitting issues with large vibrators (>10 t); hence, lighter sources might be required. Potential additional resources further south and increased geological knowledge of the area will have consequences on the mining plan and the extent to which this can be done in the area.

CONCLUSIONS

In June 2022, a novel seismic survey was conducted in Blötberget to assess the capability of combining both broadband sources and receivers in hardrock settings. The data acquisition was conducted over a well-known deposit and incorporated a combination of co-located micro-electromechanical sensors (MEMS), 3C geophones, and surface and borehole distributed acoustic sensing (DAS) measurements, alongside a broadband seismic vibrator. This case study focused on the data recorded by the MEMS, combined with borehole DAS measurements to extract a 1D velocity profile used for migration and time-to-depth conversion. The quality of the dataset was compared to the recordings of the vertical component of the 3C geophone-based receivers in terms of the amplitude spectral content. The MEMS data proved to be superior both in bandwidth and signal-to-noise ratio. The acquired MEMS data were processed using a tailored workflow to retain its broad bandwidth and provided a high-resolution image of the iron oxide deposits and its host rocks.

Most reflections imaged in this study were also present in the previous work; however, the reflection cross-cutting the mineralization shows here a reversed polarity compared to the wavelet of the first breaks, uncovering a zone of low impedance in the host rock. Given the apparent truncation of the mineralization at their intersection and the opposite dip of this cross-cutting reflection with respect to the mineralization, we suggest that this low impedance might originate from a weak zone and therefore supports previous

interpretations for this reflection to originate from a fault zone. Several near-surface reflections correspond to lithological boundaries between intrusive and volcanic rocks, with one of them showing an association with a weak magnetic lineament. Two new deeper reflections below the interpreted fault and mineralization could correspond to potential additional resources. Improved survey length towards the south and drilling through those new reflections would be necessary to understand their true nature, gain insights into the tectonic history of the study area and uncover new target regions both in the south and north of the profile.

Leveraging insights from previous seismic studies in Blötberget, the broadband data have facilitated improved imaging of the known deposits, along with the interpretation of potential additional resources in the footwall and further towards the south of the known mineralization. However, the most significant enhancement from the broadband data comes from its ability to provide the most convincing image of the cross-cutting fault. This case study underscores the potential of broadband data for achieving high-resolution subsurface imaging in hardrock environments and its role in fostering a more efficient approach to mineral resource assessment in the context of our rapidly evolving era of green technologies and decarbonization.

ACKNOWLEDGEMENTS

This study was carried out within the FUTURE project, Fiber-optic sensing and UAV-platform techniques for improved mineral exploration. FUTURE has received funding from ERA-MIN3, Raw Materials for the Sustainable Development and the Circular Economy under the Vinnova grant no. 2022-00073, which covered the Swedish partners' part. In-kind supports through time commitments for a number of co-authors from Uppsala University and Nordic Iron Ore are provided by the Smart Exploration Research Center. The Smart Exploration Research Centre has received funding from the Swedish Foundation for Strategic Research (SSF) under grant agreement no. CMM22-0003. This is publication SE24-006. We thank Emma Bäckström and Monica Schön from Nordic Iron Ore for their collaboration on the project. We thank several PhD students and post-doctoral researchers from Uppsala University, the University of the Witwatersrand and Politecnico di Torino for taking part in the seismic survey. We thank an anonymous reviewer along with the editors for their constructive comments and input.

DATA AVAILABILITY STATEMENT

The data that support the findings of this study are available from the corresponding author upon reasonable request.

ORCID

Lea Gyger https://orcid.org/0000-0002-3179-5286
Alireza Malehmir https://orcid.org/0000-0003-1241-2988
Musa Manzi https://orcid.org/0000-0002-1654-5211

REFERENCES

Allen, R.L., Lundstrom, I., Ripa, M. & Christofferson, H. (1996) Facies analysis of a 1.9 Ga, continental margin, back-arc, felsic caldera province with diverse Zn-Pb-Ag-(Cu-Au) sulfide and Fe oxide deposits, Bergslagen region, Sweden. *Economic Geology*, 91(6), 979–1008. https://doi.org/10.2113/gsecongeo.91.6.979

Almqvist, B.S., Björk, A., Mattsson, H.B., Hedlund, D., Gunnarsson, K., Malehmir, A., Högdahl, K., Bäckström, E. & Marsden, P. (2019) Magnetic characterisation of magnetite and hematite from the Blötberget apatite–iron oxide deposits (Bergslagen), south-central Sweden. *Canadian Journal of Earth Sciences*, 56(9), 948–957. https://doi.org/10.1139/cjes-2018-0183

Balestrini, F., Draganov, D., Malehmir, A., Marsden, P. & Ghose, R. (2020) Improved target illumination at Ludvika mines of Sweden through seismic-interferometric surface-wave suppression. *Geophysical Prospecting*, 68(1), 200–213. https://doi.org/10.1111/1365-2478.12890

Bastani, M. & Johansson, H. (2022) A new data acquisition system for UAV-borne VLF-LF measurements. Two case studies in Sweden. In: *NSG2022 3rd Conference on Airborne, Drone and Robotic Geophysics*, volume 2022. Houten, the Netherlands: European Association of Geoscientists & Engineers, pp. 1–5. https://doi.org/10.3997/2214-4609.202220068

Bellefleur, G., Schetselaar, E., Wade, D., White, D., Enkin, R. & Schmitt, D.R. (2020) Vertical seismic profiling using distributed acoustic sensing with scatter-enhanced fibre-optic cable at the Cu–Au new Afton porphyry deposit, British Columbia, Canada. *Geophysical Prospecting*, 68(1), 313–333. https://doi.org/10.1111/1365-2478.12828

Bräunig, L., Buske, S., Malehmir, A., Bäckström, E., Schön, M., & Marsden, P. (2020) Seismic depth imaging of iron-oxide deposits and their host rocks in the Ludvika mining area of central Sweden. *Geophysical Prospecting*, 68(1), 24–43. https://doi.org/10.1111/1365-2478.12836

Brodic, B. (2017) *Three-component digital-based seismic landstreamer: Methodologies for infrastructure planning applications*. PhD thesis, Acta Universitatis Upsaliensis.

Correa, J., Egorov, A., Tertyshnikov, K., Bona, A., Pevzner, R., Dean, T., Freifeld, B. & Marshall, S. (2017) Analysis of signal to noise and directivity characteristics of DAS VSP at near and far offsets—a CO2CRC Otway project data example. *The Leading Edge*, 36(12), 994a1–994a7. https://doi.org/10.1190/tle36120994a1.1

Correa, J., Isaenkov, R., Yavuz, S., Yurikov, A., Tertyshnikov, K., Wood, T., Freifeld, B.M. & Pevzner, R. (2021) Distributed acoustic sensing/surface orbital vibrator: rotary seismic sources with fiber-optic sensing facilitates autonomous permanent reservoir monitoring. *Geophysics*, 86(6), P61–P68. https://doi.org/10.1190/geo2020-0612.1

Cuny, T., Bettinelli, P., Le Calvez, J., Parker, R., Guerra, R. & Williams, M. (2020) Variable gauge length processing: DAS VSP examples. In: *First EAGE Workshop on Fibre Optic Sensing*, volume 1. Houten, the Netherlands: European Association of Geoscientists & Engineers, pp. 1–5. https://doi.org/10.3997/2214-4609.202030008

Daley, T.M., Miller, D., Dodds, K., Cook, P. & Freifeld, B. (2016) Field testing of modular borehole monitoring with simultaneous distributed acoustic sensing and geophone vertical seismic profiles at

Citronelle, Alabama. *Geophysical Prospecting*, 64(5), 1318–1334. https://doi.org/10.1111/1365-2478.12324

Denis, M., Brem, V., Pradalie, F., Moinet, F., Retailleau, M., Langlois, J., Bai, B., Taylor, R., Chamberlain, V. & Frith, I. (2013) Can land broadband seismic be as good as marine broadband?. *The Leading Edge*, 32(11), 1382–1388. https://doi.org/10.1190/tle32111382.1

Ding, Y. & Malehmir, A. (2021) Reverse time migration (RTM) imaging of iron oxide deposits in the Ludvika mining area, Sweden. *Solid Earth*, 12(8), 1707–1718. https://doi.org/10.5194/se-12-1707-2021

Götz, J., Lüth, S., Henninges, J. & Reinsch, T. (2018) Vertical seismic profiling using a daisy-chained deployment of fibre-optic cables in four wells simultaneously–case study at the Ketzin carbon dioxide storage site. *Geophysical Prospecting*, 66(6), 1201–1214. https://doi.org/10.1111/1365-2478.12638

Hartog, A.H. (2017) *An introduction to distributed optical fibre sensors*. Boca Raton, FL: CRC Press. https://doi.org/10.1201/9781315119014

Hloušek, F., Malinowski, M., Bräunig, L., Buske, S., Malehmir, A., Markovic, M., Sito, L., Marsden, P. & Bäckström, E. (2022) Three-dimensional reflection seismic imaging of the iron oxide deposits in the Ludvika mining area, Sweden, using Fresnel volume migration. *Solid Earth*, 13(5), 917–934. https://doi.org/10.5194/se-13-917-2022

Hons, M., Stewart, R., Lawton, D., Bertram, M. & Hauer, G. (2008) Field data comparisons of MEMS accelerometers and analog geophones. *The Leading Edge*, 27(7), 896–903. https://doi.org/10.1190/1.2954030

Jonsson, E., Troll, V.R., Högdahl, K., Harris, C., Weis, F., Nilsson, K.P. & Skelton, A. (2013) Magmatic origin of giant 'Kiruna-type' apatite-iron-oxide ores in central Sweden. *Scientific Reports*, 3(1), 1644. https://doi.org/10.1038/srep01644

Kearey, P., Brooks, M. & Hill, I. (2002) *An introduction to geophysical exploration*, volume 4. Hoboken, NJ: John Wiley & Sons. https://doi.org/10.1029/2003EO120005

Kuvshinov, B. (2016) Interaction of helically wound fibre-optic cables with plane seismic waves. *Geophysical Prospecting*, 64(3), 671–688. https://doi.org/10.1111/1365-2478.12303

Li, Y., Karrenbach, M. & Ajo-Franklin, J.B. (2021) A literature review: Distributed acoustic sensing (DAS) geophysical applications over the past 20 years. In: *Distributed acoustic sensing in geophysics: Methods and applications*. Washington, DC: American Geophysical Union, pp. 229–291. https://doi.org/10.1002/9781119521808.ch17

Malehmir, A., Durrheim, R., Bellefleur, G., Urosevic, M., Juhlin, C., White, D.J., Milkereit, B. & Campbell, G. (2012) Seismic methods in mineral exploration and mine planning: a general overview of past and present case histories and a look into the future. *Geophysics*, 77(5), WC173–WC190. https://doi.org/10.1190/geo2012-0028.1

Malehmir, A., Dynesius, L., Paulusson, K., Paulusson, A., Johansson, H., Bastani, M., Wedmark, M. & Marsden, P. (2017) The potential of rotary-wing UAV-based magnetic surveys for mineral exploration: a case study from central Sweden. *The Leading Edge*, 36(7), 552–557. https://doi.org/10.1190/tle36070552.1

Malehmir, A., Maries, G., Bäckström, E., Schön, M. & Marsden, P. (2017) Developing cost-effective seismic mineral exploration methods using a landstreamer and a drophammer. *Scientific Reports*, 7(1), 10325. https://doi.org/10.1038/s41598-017-10451-6

Malehmir, A., Markovic, M., Marsden, P., Gil, A., Buske, S., Sito, L., Bäckström, E., Sadeghi, M. & Luth, S. (2021) Sparse 3D reflection seismic 33survey for deep-targeting iron oxide deposits and their host rocks, Ludvika mines, Sweden. *Solid Earth*, 12(2), 483–502. https://doi.org/10.5194/se-12-483-2021

Malehmir, A., Markovic, M., Papadopoulo, M. & Marsden, P. (2023) Establishment of a hardrock seismic test site in central Sweden. Paper presented at the KEGS Symposium, Toronto, Canada, March 2023. https://doi.org/10.6084/m9.figshare.22215514.v1

Malehmir, A., Markovic, M., Papadopoulou, M., Högdahl, K., Ask, M., Strømme, M., Pitcairn, I., Martin, T., Zack, T., Majka, J., et al,. (2024) Smart exploration research centre: knowledge and innovation for exploration of critical raw materials. *First Break*, 42(8), 89–93.

Manzi, M., Durrheim, R. & Cooper, G. (2018) 3D conventional vs 3D broadband reflection seismics for deep mineral exploration: Re-process legacy data or re-acquire n. In: *80th EAGE Conference and Exhibition 2018*, volume 2018, Houten, the Netherlands: European Association of Geoscientists & Engineers, pp. 1–5.

Maries, G., Malehmir, A., Bäckström, E., Schön, M. & Marsden, P. (2017) Downhole physical property logging for iron oxide exploration, rock quality, and mining: an example from central Sweden. *Ore Geology Reviews*, 90, 1–13. https://doi.org/10.1016/j.oregeorev.2017.10.012

Maries, G., Malehmir, A. & Marsden, P. (2020) Cross-profile seismic data acquisition, imaging, and modeling of iron oxide deposits: a case study from Blötberget, south-central Sweden. *Geophysics*, 85(6), B233–B247. https://doi.org/10.1190/geo2020-0173.1

Markovic, M., Maries, G., Malehmir, A., von Ketelhodt, J., Bäckström, E., Schön, M. & Marsden, P. (2020) Deep reflection seismic imaging of iron-oxide deposits in the Ludvika mining area of central Sweden. *Geophysical Prospecting*, 68(1), 7–23. https://doi.org/10.1111/1365-2478.13340

Mougenot, D., Cherepovskiy, A. & JunJie, L. (2011) MEMS-based accelerometers: expectations and practical achievements. *First Break*, 29(2), 85–90. https://doi.org/10.3997/1365-2397.20112st4

Mougenot, D. & Thorburn, N. (2004) MEMS-based 3D accelerometers for land seismic acquisition: Is it time? *The Leading Edge*, 23(3), 246–250.

Nanda, N.C. (2021) Seismic reflection principles-basics. In: *Seismic data interpretation and evaluation for hydrocarbon exploration and production: A practitioner's guide* . Cham: Springer, pp 19–35.

Noorlandt, R., Drijkoningen, G., Dams, J. & Jenneskens, R. (2015) A seismic vertical vibrator driven by linear synchronous motors. *Geophysics*, 80(2), EN57–EN67.

Nordic Iron Ore. (2011) Ludvika mines preliminary economic assessment. Final Report. Rev, 3, 1–74.

Nordic Iron Ore. (2019) Blötberget feasibility report. Golder, Executive Summary, 5. Accessed: 2023-12-15. https://nordicironore.se/wp-content/uploads/2019/10/executive-summary.pdf

Papadopoulou, M., Da Col, F., Mi, B., Bäckström, E., Marsden, P., Brodic, B., Malehmir, A. & Socco, L.V. (2020) Surface-wave analysis for static corrections in mineral exploration: a case study from central Sweden. *Geophysical Prospecting*, 68(1), 214–231. https://doi.org/10.1111/1365-2478.12895

Pertuz, T., Malehmir, A., Bos, J., Brodic, B., Ding, Y., de Kunder, R. & Marsden, P. (2021) Broadband seismic source data acquisition and processing to delineate iron oxide deposits in the Blötberget mine, central Sweden. *Geophysical Prospecting*, 70(1), 79–94. https://doi.org/10.1111/1365-2478.13159

Riedel, M., Cosma, C., Enescu, N., Koivisto, E., Komminaho, K., Vaittinen, K., & Malinowski, M. (2018) Underground vertical seismic profiling with conventional and fiber-optic systems for exploration in the Kylylahti polymetallic mine, Eastern Finland. *Minerals*, 8(11), 538. https://doi.org/10.3390/min8110538

SGU. (2014) Rikstäckande jorddjupsmodell. SGU-rapport 2014:14, Uppsala, Sweden: Sveriges Geologiska Undersökning.

SGU. (2018) Berggrund. map. Uppsala, Sweden: Sveriges Geologiska Undersökning. Scale 1:50 000-1:250 000.

Stephens, M., Ripa, M., Lundström, I., Persson, L., Bergman, T., Ahl, M., Wahlgren, C.-H., Persson, P.-O. & Wickström, L. (2009) *Synthesis of bedrock geology in the Bergslagen region, Fennoscandian Shield, south-central Sweden*, volume v. 58. Uppsala, Sweden: Sveriges geologiska undersökning (SGU).

Tellier, N. & Lainé, J. (2017) Understanding mems-based digital seismic sensors. *First Break*, 35(1), 93–100. https://doi.org/10.3997/1365-2397.35.1.87386

Ten Kroode, F., Bergler, S., Corsten, C., de Maag, J.W., Strijbos, F. & Tijhof, H. (2013) Broadband seismic data—the importance of low frequencies. *Geophysics*, 78(2), WA3–WA14. https://doi.org/10.1190/geo2012-0294.1

Willis, M.E. (2022) *Distributed acoustic sensing for seismic measurements–What geophysicists and engineers need to know*. Houston, TX: Society of Exploration Geophysicists. https://doi.org/10.1190/1.9781560803850

Yehuwalashet, E. & Malehmir, A. (2018) Gravity and magnetic survey, modeling and interpretation in the blötberget iron-oxide mining area of central Sweden. In *SEG International Exposition and Annual Meeting*. Houston, TX: SEG, pp. SEG–2018. https://doi.org/10.1190/segam2018-2992225.1

How to cite this article: Gyger, L., Malehmir, A., Manzi, M., Vivin, L., Lépine, J., Kaslilar, A. et al. (2025) Broadband seismic data acquisition and processing of iron oxide deposits in Blötberget, Sweden. *Geophysical Prospecting*, 73, 80–95. https://doi.org/10.1111/1365-2478.13648